JOURNAL OF SOLID STATE CHEMISTRY 116, 364–368 (1995)

A Mo(IV) Monophosphate, $BaMo(PO_4)_2$, with the Yavapaiite Layer Structure

A. Leclaire, M. M. Borel, J. Chardon, and B. Raveau

Laboratoire CRISMAT, ISMRA et Université de Caen, 6 Boulevard du Maréchal Juin, 14050 Caen Cédex, France

Received June 27, 1994; in revised form November 7, 1994; accepted November 10, 1994

A new molybdenum monophosphate $BaMo(PO_4)_2$ with the yavapaiite structure has been synthesized and its structure was determined from a single crystal. This is the first phase of this family characterized by a reduced oxidation state of the transition element, i.e., Mo(IV). This layer monophosphate that crystallizes in the $C2/m$ space group with $a = 8.211(1)$, $b = 5.2757(6)$, $c = 7.816(2)$ Å, $\beta = 94.778(1)^\circ$ exhibits close relationships with the tridimensional framework of β-cristoballite, α-$NaTiP_2O_7$, and $CsMoOP_2O_7$.

INTRODUCTION

The recent investigations of transition element phosphates have shown the possibility to synthesize numerous compounds in which the transition metal exhibits a reduced oxidation state. This is particularly the case of the molybdenophosphates of the systems A–Mo–P–O with A = Na, K, Rb,Cs, for which original mixed frameworks involving either Mo(V), Mo(IV), Mo(III), or mixed valencies of molybdenum have been isolated (see for instance for a review Ref. 1). Contrary to the alkaline phosphates, alkaline earth phosphates and especially barium molybdenophosphates have not been extensively studied up to date. The only barium compounds that have been isolated are the $BaMo_2P_3O_{12}$ (2), $BaMo_2P_4O_{14}$ (3), $BaMo_2P_4O_{16}$ (4), and $BaMo_4P_2O_{16}$ (5).

For this reason, the system Ba–Mo(IV)–P–O has been reinvestigated. This paper reports on the synthesis and crystal structure of a new monophosphate $BaMo(PO_4)_2$ that exhibits the layered structure of the monoclinic aluns of the yavapaiite type (6, 7), also described for the phosphotitanate $BaTi(PO_4)_2$, by Masse and Durif (8). Structural relationships between the layer structure of yavapaiite and the tridimensional framework of β-cristoballite, nasicon, and of the phosphates α-$NaTiP_2O_7$ (9) and $CsMoOP_2O_7$ (10) are also studied.

SYNTHESIS

The growth of single crystals of $BaMo(PO_4)_2$ was performed in two steps starting from a mixture of nominal composition $Ba_3Mo_4P_6O_{24}$. First an adequate mixture of $BaCO_3$, $(NH_4)_2HPO_4$ and MoO_3 was heated at 973 K in a platinum crucible to eliminate CO_2, H_2O, and NH_3. In the second step, the appropriate amount of molybdenum (1 mole) was added and the finely ground product sealed in an evacuated ampoule was heated up to 1173 K for 12 h and then quenched to room temperature.

Two sorts of crystals were extracted from the resulting product: mauve crystals and yellow crystals; the microprobe analysis of the first kind of crystals confirmed the composition $BaMo(PO_4)_2$ deduced from the structure determination. The microprobe analysis of the yellow crystals revealed a new molybdenum phosphate involving barium but unfortunately the poor quality of the crystals did not allow their structure to be determined up to now. Subsequently a reaction to prepare pure powder $BaMo(PO_4)_2$ was carried out at 1173 K for 12 hr, quenching the sample to room temperature. The powder X ray diffraction pattern (Table 1) of this new phosphate was indexed in a monoclinic cell (Table 2) in agreement with the parameters obtained from the single-crystal X ray study.

STRUCTURE DETERMINATION

A mauve crystal with dimensions $0.071 \times 0.038 \times 0.038$ mm was selected for the structure determination. The cell parameters reported in Table 2 were determined and refined by diffractometric techniques at 294 K with a least squares refinement based upon 25 reflections with $18^\circ \leq \theta \leq 22^\circ$. The data were collected on a CAD4 Enraf-Nonius diffractometer with the data collection parameters of Table 2. The reflections were corrected for Lorentz, polarization, and absorption effects. The systematic absences

0022-4596/95 $6.00

TABLE 1
X Ray Powder Diffraction Data of $BaMo(PO_4)_2$

h	k	l	d_{obs}(Å)	d_{calc}(Å)	I/I_o
0	0	1	7.800	7.788	3
1	1	0	4.437	4.434	89
2	0	0	4.096	4.091	77
0	0	2	3.900	3.894	34
1	1	1	3.775	3.781	44
2	0	$\bar{1}$	3.756	3.753	21
2	0	1	3.511	3.504	10
1	1	$\bar{2}$	2.998	2.994	100
2	0	$\bar{2}$	2.948	2.946	11
1	1	2	2.863	2.863	58
2	0	2	2.712	2.710	14
0	2	0	2.640	2.638	54
0	0	3	2.597	2.596	6
3	1	0	2.424	2.423	66
2	0	$\bar{3}$	2.272	2.279	3
3	1	1		2.266	·
2	2	0	2.220	2.217	11
0	2	2	2.185	2.184	27
2	2	$\bar{1}$	2.158	2.159	9
3	1	$\bar{2}$	2.129	2.129	20
4	0	0	2.045	2.045	10
3	1	2	1.993	1.992	8
2	2	$\bar{2}$	1.966	1.965	24
0	0	4	1.948	1.947	10
2	2	2	1.892	1.890	20
4	0	$\bar{2}$	1.876	1.876	8
3	1	$\bar{3}$	1.838	1.840	4
2	0	$\bar{4}$	1.819	1.818	19
1	1	4	1.755	1.754	25
4	0	2		1.752	
1	3	0	1.720	1.719	16
4	2	0	1.616	1.616	2
1	3	$\bar{2}$	1.583	1.583	20
0	2	4	1.564	1.566	19
5	1	0		1.563	
1	3	2		1.563	
4	2	$\bar{2}$	1.529	1.529	11
2	0	$\bar{5}$	1.497	1.498	11
2	2	$\bar{4}$		1.497	
3	3	0	1.478	1.478	24

$h + k = 2n + 1$ for all hkl are consistent with the $C2$, Cm, or $C2/m$ space group. The atoms were located by the heavy atom method and successfully refined in the centrosymmetric space group $C2/m$. The positional and thermal parameters for $BaMo(PO_4)_2$ listed in Table 3 lead to the factors $R = 0.030$ and $R_w = 0.036$.

RESULTS AND DISCUSSION

The projection of the structure of $BaMo(PO_4)_2$ onto the (010) plane (Fig. 1) shows the layered character previously found for the alun sulfates (6, 7). It consists of very simple $[MoP_2O_8]_\infty$ layers built up from corner-sharing PO_4 tetrahedra and MoO_6 octahedra, and interleaved with barium

TABLE 2
Summary of Crystal Data Intensity, Measurements and Structure Refinement Parameters for $BaMo(PO_4)_2$

1. Crystal data	
Space group	$C2/m$
Cell dimensions	$a = 8.211(1)$ Å
	$b = 5.2757(6)$ $\beta = 94.77(1)°$
	$c = 7.816(2)$
Volume (Å)^3	337.4(2)
Z	2
ρ_{calc} (gcm^3)	4.17
2. Intensity measurements	
λ(Mo$K\alpha$)	0.71073
Scan mode	ω
Scan width (°)	$1.3 + 0.35 \tan\theta$
Slit aperture (mm)	$1.4 + \tan\theta$
Max θ(°)	45
Standard reflections	3 measured every 3600 sec
Measured reflections	1554
Reflections with $I > 3\sigma$	801
μ(mm^{-1})	8.09
3. Structure solution and refinement	
Parameters refined	37
Agreement factors	$R = 0.030$ $R_w = 0.036$
Weighting scheme	$w = f(\sin\theta/\lambda)$
Δ/σ max	<0.004

cations. Note that each PO_4 tetrahedron exhibits one free apex pointing out of the layer.

Each MoO_6 octahedron shares its six apices with PO_4 tetrahedra as shown from the projection of one layer onto the (001) plane (Fig. 2). Reciprocally, each PO_4 tetrahedron is linked to three MoO_6 octahedra. As a result each PO_4 tetrahedron exhibits three identical P–O distances corresponding to the P–O–Mo bonds, i.e., to O(1) and O(2), and a shorter P–O bond corresponding to the free apex O(3) (Table 4). The Mo–O distances of the MoO_6 octahedron (Table 4) are similar to those observed for other Mo(IV) monophosphates. Note however, that the geometry of the MoO_6 octahedron is very similar to that

TABLE 3
Positional Parameters and Their Estimated Standard Deviations

Atom	x	y	z	B(A2)
Ba	0.	0.	0.	1.309(6)
Mo	0.	0.	0.5	0.856(8)
P	0.1294(2)	0.5	0.2899(2)	0.88(2)
O(1)	0.0242(4)	0.2610(6)	0.3123(4)	1.29(4)
O(2)	0.2652(5)	0.5	0.4392(6)	1.21(6)
O(3)	0.1862(6)	0.5	0.1122(6)	1.65(7)

Note. Anisotropically refined atoms are given in the form of the isotropic equivalent displacement parameter defined as

$$B = (4/3) \sum_i \sum_j \vec{a}_i \cdot \vec{a}_j \beta_{ij}.$$

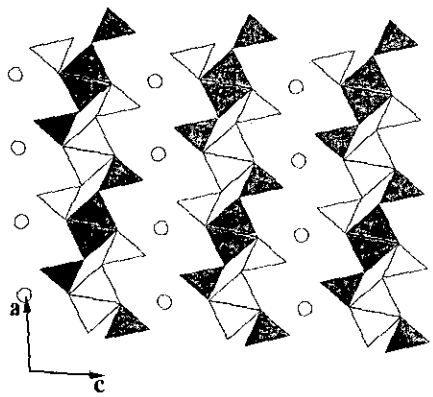

FIG. 1. Projection of the $BaMo(PO_4)_2$ structure along [010].

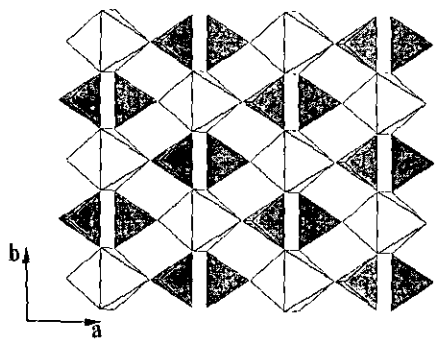

FIG. 2. Projection of a $[MoP_2O_8]_\infty$ layer onto the [001] plane.

of the FeO_6 octahedron in the mineral yavapaiite (7); one indeed observed in both cases a flattening of this polyhedron leading to two short Mo(Fe)–O bonds (1.947–1.954 Å) and four larger ones (2.00–2.034 Å).

The barium cation is linked to four O(1) atoms located within the $[MoP_2O_8]_\infty$ layer and to two O(3) atoms corresponding to the free apices of the PO_4 tetrahedra. Like potassium in the yavapaiite, barium exhibits an octahedral coordination. However, the BaO_6 octahedron, with six Ba–O distances ranging from 2.79 to 2.795 Å (Table 4), is remarkably regular (Fig. 3) compared to the KO_6 octahedron (2.826 to 2.860 Å). It appears as one of the most

TABLE 4
Distances (Å) and Angles (°) in the Polyhedra

Mo	$O(1^{i})$	$O(1)$	$O(1^{ii})$	$O(1^{iii})$	$O(2^{iv})$	$O(2^{v})$
$O(1^{i})$	2.034(3)	4.067(7)	2.754(7)	2.994(7)	2.846(5)	2.784(5)
O(1)	180	2.034(3)	2.994(7)	2.754(7)	2.784(5)	2.846(5)
$O(1^{ii})$	85.2(2)	94.8(2)	2.034(3)	4.067(7)	2.846(5)	2.784(5)
$O(1^{iii})$	94.8(2)	85.2(2)	180	2.034(3)	2.784(5)	2.846(5)
$O(2^{iv})$	88.7(2)	91.3(1)	88.7(2)	91.3(2)	1.947(4)	3.894(7)
$O(2^{v})$	91.3(2)	88.7(2)	91.3(2)	88.7(2)	180	1.947(4)
P	O(1)	$O(1^{vi})$	O(2)	O(3)		
O(1)	1.547(4)	2.522(7)	2.483(5)	2.480(5)		
$O(1^{vi})$	109.2(3)	1.547(4)	2.483(5)	2.480(5)		
O(2)	106.8(2)	106.8(2)	1.546(5)	2.584(7)		
O(3)	108.9(2)	108.9(2)	116.0(3)	1.501(5)		
			Ba–$O(1^{vii})$ = 2.795(4)			
			O(1) = 2.795(4)			
			$O(1^{iii})$ = 2.795(4)			
			$O(1^{viii})$ = 2.795(4)			
			$O(3^{iv})$ = 2.790(5)			
			$O(3^{ix})$ = 2.790(5)			

Symmetry code
(i) $-x, -y, 1-z$
(ii) $-x, y, 1-z$
(iii) $x, -y, z$
(iv) $x-1/2, y-1/2, z$
(v) $1/2-x, 1/2-y, 1-z$
(vi) $x, 1-y, z$
(vii) $-x, -y, -z$
(viii) $-x, y, -z$
(ix) $1/2-x, 1/2-y, -z$

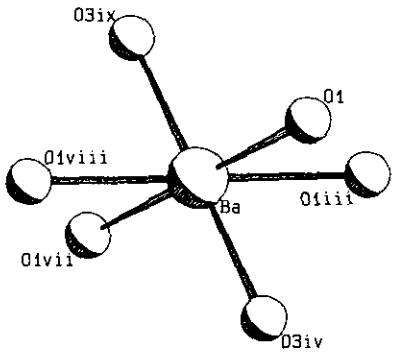

FIG. 3. The oxygen polyhedron around Ba.

regular octahedra encountered in the $AM(XO_4)_2$ structures. Moreover, the next nearest oxygen neighbors are located at much larger distances (>3.5 Å), contrary to potassium in the yavapaiite structure that exhibits three additional neighbors at 3.12 Å.

Many compounds with the generic formulation $AM(XO_4)_2$ with X = S, Se, Cr, Mo, W, and P have been synthesized up to date. Most of them exhibit a layer structure with close relationships that have lead to an interesting structural classification (11). In this classification the yavapaiite structure, and consequently $BaMo(PO_4)_2$, belongs to category II; i.e., it can be considered as the less distorted structure with respect to the highest symmetry $P\bar{3}ml$ observed for the class I compounds. Thus the $[MoP_2O_8]_\infty$ layers (Fig. 2) derive from the ideal trigonal layers (Fig. 4) of $KAl(MoO_4)_2$ (12) by a rotation of the PO_4 tetrahedra around axis located within the layer as already described (11).

The most interesting feature leads with the close relationships between the layer structure of the $AM(XO_4)_2$ compounds and the tridimensional structures of α-$NaTiP_2O_7$ (9) and consequently of β-cristoballite. Considering the view of the $BaMo(PO_4)_2$ structure along b (Fig. 1), a tridimensional framework $[MoP_2O_8]_\infty$ similar to that of α-$NaTiP_2O_7$ (Fig. 5) can be obtained by translating two successive $[MoP_2O_8]_\infty$ layers of $((\vec{a}/3) + (\vec{c}/5))$ with respect

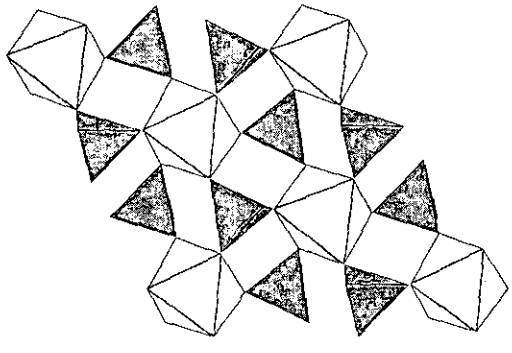

FIG. 4. The $[TiP_2O_8]_\infty$ layer in α-$NaTiP_2O_7$.

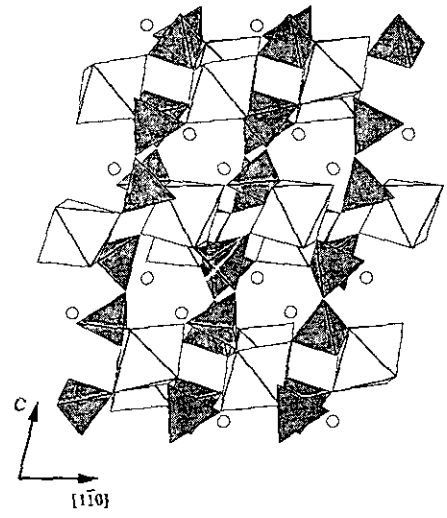

FIG. 5. The projection of the α-$NaTiP_2O_7$ structure along [110] showing the octahedral layers and the P_2O_7 layers.

to each other and by connecting the PO_4 tetrahedra of these two layers. In this way, the $[MoP_2O_7]_\infty$ framework consists, like the $[TiP_2O_7]_\infty$ framework, of octahedral layers connected through layers of diphosphate groups. It results in distorted hexagonal tunnels with a disposition very similar to that of β-cristoballite (Fig. 6). In fact the $BaMo(PO_4)_2$ structure differs mainly from the α-$NaTiP_2O_7$ structure by the distortion of the $[MoP_2O_8]_\infty$ layers (Fig. 2). The α-$NaTiP_2O_7$ structure can indeed be described as the stacking of mixed $[TiP_2O_8]_\infty$ layers absolutely similar to the $[AlMo_2O_8]_\infty$ (Fig. 4) encountered in the molybdate $KAl(MoO_4)_2$ (12), i.e., built up from corner-sharing TiO_6 octahedra and PO_4 tetrahedra with the $P\bar{3}1m$ symmetry. In summary, the $KAl(MoO_4)_2$ layer structure (class I) derives from the α-$NaTiP_2O_7$ structure by a simple sharing mechanism at the level of the bridging oxygen of the P_2O_7 groups leading to the formation of single MoO_4 tetrahedra (instead of MoO_2 groups), whereas in the $BaMo(PO_4)_2$ structure (class II), the sharing mechanism at the level of

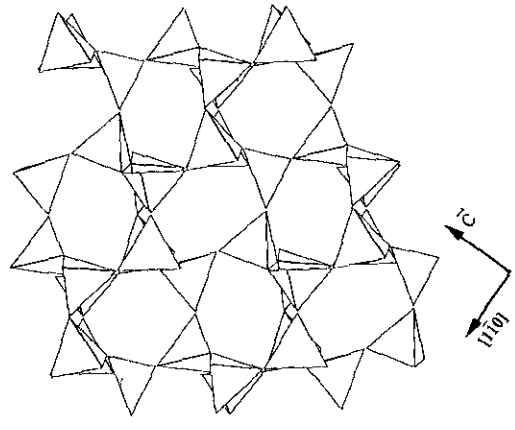

FIG. 6. The projection of the β-cristoballite structure along [110].

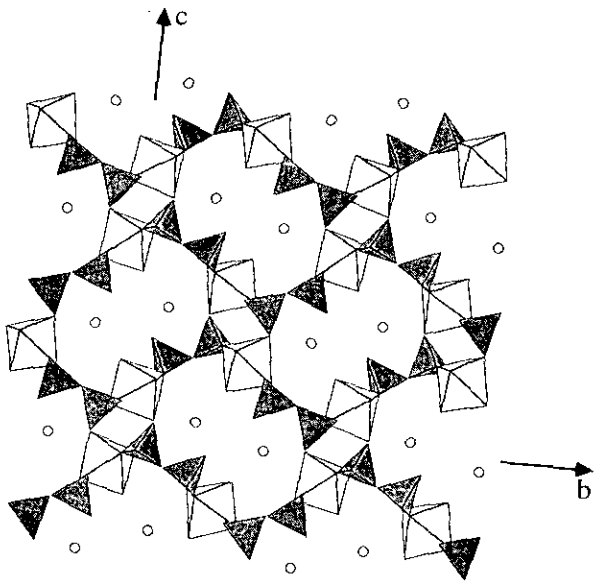

FIG. 7. Projection of the structure of $CsMoP_2O_8$ along $\vec{a}$.

the bridging oxygen is followed by a distortion of the $[MoP_2O_8]_\infty$ layers.

The close relationships that have been previously established between α-$NaTiP_2O_7$ and β-cristoballite (9) make obvious the structural filiation between these different compounds. Let us indeed recall that the α-$NaTiP_2O_7$ structure derives from the β-cristoballite structure by replacing one (111) layer of P_2O_7 groups out of two by one layer of TiO_6 octahedron (compare Figs. 5 and 6).

The close relationships between the $CsMoOP_2O_7$ (10) and α-$NaTiP_2O_7$ (9) structures, which both consist of the stacking of similar layers of P_2O_7 groups with layers of TiO_6 (or MoO_6) octahedra, show that the layer structures $AM(XO_4)_2$ are also closely related to the tridimensional framework of $CsMoOP_2O_7$ (Fig. 7). Nevertheless, it must be pointed out that in the latter, the P_2O_7 groups exhibit a staggered configuration contrary to α-$NaTiP_2O_7$ so that the orientations of the successive octahedral layers are different in the two structures.

In conclusion, the Mo(IV) monophosphate $BaMo(PO_4)_2$ is the only one that involves a reduced oxidation state of the transition element among all the compounds $AM(XO_4)_2$ related to the yavapaiite structure. This feature and the close relationships with the tridimensional structures of β-cristoballite and α-$NaTiP_2O_7$ open the route to research of other phosphates related to this family.

REFERENCES

1. R. C. Haushalter and L. A. Mundi, *Chem. Mater.* **4,** 31 (1992).
2. A. Leclaire, M. M. Borel, A. Grandin, and B. Raveau, *Eur. J. Solid State Inorg. Chem.* **26,** 45 (1989).
3. A. Leclaire, J. Chardon, M. M. Borel, A. Grandin, and B. Raveau, *Z. Anorg. Allg. Chem.* **617,** 127 (1992).
4. G. Costentin, M. M. Borel, A. Grandin, and B. Raveau, *J. Solid State Chem.* **89,** 83 (1990).
5. M. M. Borel, J. Chardon, A. Leclaire, A. Grandin, and B. Raveau, *J. Solid State Chem.* **112,** 317 (1994).
6. C. O. Hutton, *Am. Miner.* **44,** 1105 (1959).
7. E. J. Graeber and A. Rosenzweig, *Am. Miner.* **56,** 1917 (1971).
8. R. Masse and A. Durif, *C.R. Acad. Sci. Paris, Sér. C* **274,** 1692 (1972).
9. A. Leclaire, A. Benmoussa, M. M. Borel, A. Grandin, and B. Raveau, *J. Solid State Chem.* **72,** 299 (1988).
10. A. Guesdon, M. M. Borel, A. Grandin, A. Leclaire, and B. Raveau, *J. Solid State Chem.* **108,** 46 (1993).
11. S. Oyetola, A. Verbaere, Y. Piffard, and M. Tournoux, *Eur. J. Solid State Inorg. Chem.* **25,** 259 (1988).
12. R. F. Klevtsova and P. V. Klevtsov, *Kristallografiya* **15,** 953 (1970).